THE JOURNAL OF PHYSICAL CHEMISTRY B

Article

pubs.acs.org/JPCB

Dynamics and Kinetics of Structure Formation in Molecularly Tethered Fluorocarbon/Hydrocarbon Amphiphiles

M. M. Elmahdy,[†,§] C. G. Clark, Jr.,[‡] H.-J. Butt,[‡] K. Müllen,[‡] and G. Floudas*[,†,‡]

[†]Department of Physics, University of Ioannina, GR-45110, Ioannina and Foundation for Research and Technology-Biomedical Research Institute, Ioannina, Greece

[‡]Max Planck Institute for Polymer Research, D-55128 Mainz, Germany

ABSTRACT: Biphasic fluorocarbon/hydrocarbon amphiphiles tethered to cores at distances commensurate with their packing requirement can provide thermodynamic pathways toward equilibrium. This contrasts with the analogous semifluorinated alkanes. The dynamics of a fluorous biphasic hexa(3,5-substituted-phenyl)benzene (HPB) is studied with dielectric spectroscopy as a function of temperature and pressure in comparison to the parent biphasic diphenylacetylene (DPA). Dielectric spectroscopy is a sensitive probe of the fluorocarbon environment through the end C−F dipole. Four dielectrically active processes were observed that associate with the CF_3 environment within the different phases (isotropic, liquid-like lamellar, solid lamellar, glassy state). Pressure facilitates the construction of the equilibrium phase diagram. The kinetic pathways to fluorocarbon organization are explored by pressure-jump experiments. A highly cooperative process was found that is atypical of a nucleation and growth process expected for first-order transitions.

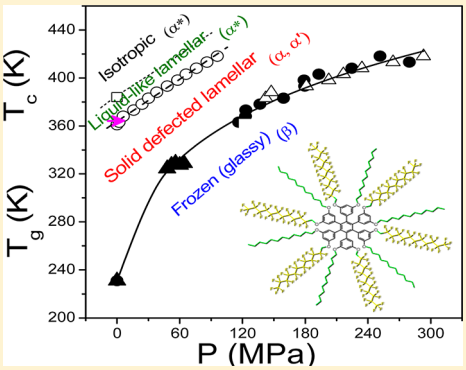

I. INTRODUCTION

Fluorinated amphiphiles constitute unique molecular building blocks for engineering structures at the nanometer scale.[1] In these materials molecular design takes advantage of the presence of fluorine. Fluorine combines electronegativity with low polarizability and can provide contrast in NMR and dielectric studies. Perfluoroalkyl chains are bulkier, have a helical structure and are much more rigid than their analogous hydrocarbon alkyl chains. Furthermore, perfluoroalkyl chains are more hydrophobic being at the same time oleophobic. Partially fluorinated compounds can enhance the self-assembly through the fluorophobic effect. The smallest such compounds are diblock copolymers of semifluorinated alkanes (SFAs), with the chemical structure $F(CF_2)_m(CH_2)_nH$ (F_mH_n).[2−12] The incompatibility and cross-sectional incommensurability of the fluorocarbon and hydrocarbon blocks favor bilayered lamellae that best minimize the hetero contacts and allow for hydrocarbon segments to adjust their density through interdigitation. However, the high-temperature phase in $F_{12}H_n$ consist of monolayers.

Biphasic fluorocarbon/hydrocarbon amphiphiles tethered to cores at distances commensurate with their packing requirement may provide thermodynamic pathways toward the equilibrium structure. In this respect, the synthesis and solid state structure of a fluorous biphasic hexa(3,5-substituted-phenyl)benzene (HPB), analogous to SFAs, was recently reported.[13] Tethering of poorly miscible hydrocarbon and fluorocarbon side chains to the rotationally flexible HPB core was shown to lead to a rich self-assembly. The structure at the mesoscopic and microscopic length scales was investigated[13] by polarizing optical microscopy (POM), X-ray scattering, and the thermodynamics by differential scanning calorimetry (DSC). In addition, ^{19}F magic-angle spinning solid state NMR was employed to probe the local environment of the CF_3 groups. In contrast to SFAs, in this propeller-like molecule, the equilibrium structure is determined not only by the propensity for phase separation between the hydrocarbon and fluorocarbon side chains but also by the ability to convert among different rotation conformational isomers. The X-ray and ^{19}F NMR studies revealed the presence of thermodynamically unfavorable yet kinetically trapped mixed conformations in the fluorous biphasic HPB. It was further shown that the addition of a minor component (∼1%) of the parent biphasic diphenylacetylene (DPA), possessing only two chains of each type at distances greater than the sums of their van der Waals radii, has a drastic effect on self-assembly. It softens the conformational barriers and unlocks the unfavorable (mixed) conformations, resulting in the formation of the thermodynamically favorable bilayer structure.

The purpose of the present investigation is to explore the dipolar dynamics in the CF_3 environment in view of the rich self-assembly. For this purpose, we employ dielectric spectroscopy (DS) and rheology. DS, in particular, is well suited in investigating the dynamics because the uncompensated end fluorine dipole of fluorinated chain is a sensitive probe of the local environment experienced by the CF_3 group. The basic

Received: September 24, 2012
Revised: October 31, 2012
Published: November 2, 2012

thermodynamic variables of temperature (T) and pressure (P) are employed and the dynamics are studied as a function of frequency and time. This enabled the construction of the first equilibrium phase diagram for a fluorous biphasic compound. In addition it allowed investigating the stability (and metastability) of phases by following the kinetic pathways to fluorocarbon self-organization.

II. EXPERIMENTAL SECTION

Synthesis. The synthesis of the biphasic hexaphenylbenzene (HPB), hexakis(3-(1- perfluoroundecylmethoxy)-5-dodecyloxyphenyl)benzene followed the general route of sequential alkylation of the two phenols of a subsituted resorcinol during the buildup of a biphasic tolane (diphenylacetylene, DPA). The complete synthetic details are presented elsewhere.[13] Scheme 1 gives the chemical structure of the investigated compounds.

Scheme 1. Chemical Structure and Molecular Packing of the Biphasic DPA and Biphasic HPB

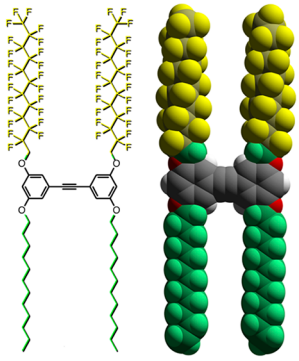

DPA

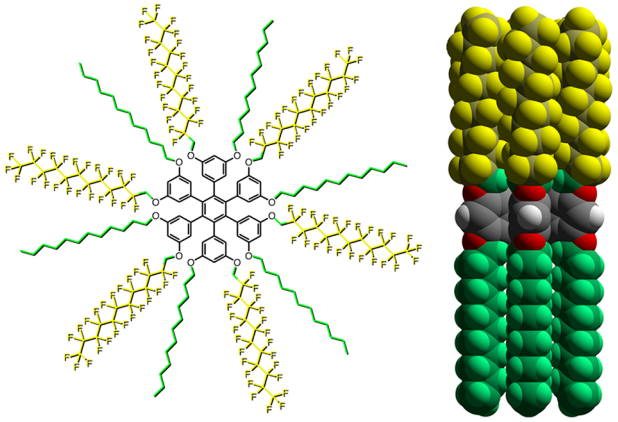

HPB

Differential Scanning Calorimetry (DSC). A Mettler Toledo Star differential scanning calorimeter (DSC) was used for the thermal measurements. The sample was first heated from ambient temperature to 423 K. A second cooling/heating experiment was made and the transition temperatures and heats of fusion were obtained during the second heating run. All runs were made with a rate of 10 K/min.

X-rays. Wide-angle X-ray scattering (WAXS) measurements were made from macroscopically oriented (extruded) filaments (at T = 298.15 K) with a diameter of 0.7 mm using pinhole collimation and a two-dimensional detector (Siemens A102647) with 1024 × 1024 pixels. OSMIC confocal optics were used for monochromatic X-ray beam (λ = 0.154 nm) and the sample-to-detector distance was 7.05 cm. Measurements were made at different temperatures on heating (295, 313, 323, 333, 343, 353, 363, and 373 K) and subsequent cooling (363, 353, 333, and 303 K). Small-angle X-ray scattering (SAXS) measurements were made from an oriented fiber using a 18 kW rotating-anode X-ray source with pinhole collimation and a two-dimensional detector with 1024 × 1024 pixels. The sample-to-detector distance was set at 1.63 m. Measurements of 1 h were made at the same temperatures as in WAXS.

Dielectric Spectroscopy (DS). Two types of experiments were performed: "isobaric" as a function of temperature and "isothermal" as a function of pressure.[14,15] The "isobaric" measurements were performed at different temperatures in the range 123.15−433.15 K, at atmospheric pressure, and for frequencies in the range from 10^{-2} to 10^{6} Hz using a Novocontrol BDS system composed of a frequency response analyzer (Solartron Schlumberger FRA 1260) and a broad-band dielectric converter. The sample cell consisted of two electrodes 20 mm in diameter and the sample with a thickness of 55 μm. The P-dependent (i.e., "isothermal") measurements were made using a setup consisting of a temperature-controlled high-pressure cell, a pump for hydrostatic pressure, and a closing press with pump. The pressure was applied using silicone oil as the transducing medium. The sample cell again consisted of two metal electrodes 20 mm in diameter with a 55 μm thick sample the spacing maintained by Teflon spacers, which was sealed and placed inside a Teflon ring to prevent contact with oil. The same BDS system as with the T-dependent measurements was used for the P-dependent measurements. "Isothermal" measurements were made for temperatures in the range 363−418 K and for pressures up to 300 MPa. Using these experiments the phase state of the system was established. Subsequently, kinetic experiments were performed by pressure-jump experiments to different final pressures favoring the formation of a new phase. In all cases, the complex dielectric permittivity $\varepsilon^* = \varepsilon' - i\varepsilon''$, where ε' is the real and ε'' is the imaginary part, was obtained as a function of frequency ω, temperature T, and pressure P, i.e., $\varepsilon^*(T,P,\omega)$. The analysis of both T- and P-dependent experiments was made using the empirical equation of Havriliak and Negami:[16]

$$\varepsilon^*(\omega) = \varepsilon_\infty + \frac{\Delta\varepsilon(T)}{[1 + (i\omega\tau_{HN}(T))^m]^n} \quad (1)$$

Here $\Delta\varepsilon(T)$ is the relaxation strength of the process under investigation, τ_{HN} is the relaxation time of the equation, m and n ($m > 0$, $mn \leq 1$) describe the symmetrical and asymmetrical broadening of the distribution of relaxation times, and ε_∞ is the dielectric permittivity at the limit of high frequencies. The relaxation times at maximum loss (τ_{max}) are presented herein and have been analytically obtained by the Havriliak−Negami equation as follows:

$$\tau_{max} = \tau_{HN} \cdot \sin^{-1/m}\left(\frac{\pi m}{2(1+n)}\right) \cdot \sin^{1/m}\left(\frac{\pi mn}{2(1+n)}\right) \quad (2)$$

At lower frequencies, ε'' rises due to the conductivity ($\varepsilon'' = \sigma/(\omega\varepsilon_f)$, where σ is the dc conductivity and ε_f is the permittivity of free space). The conductivity contribution has also been taken into account during the fitting process. The measured ε'' spectra have been used for the analysis except at high

dx.doi.org/10.1021/jp309465z | J. Phys. Chem. B 2012, 116, 13812−13820

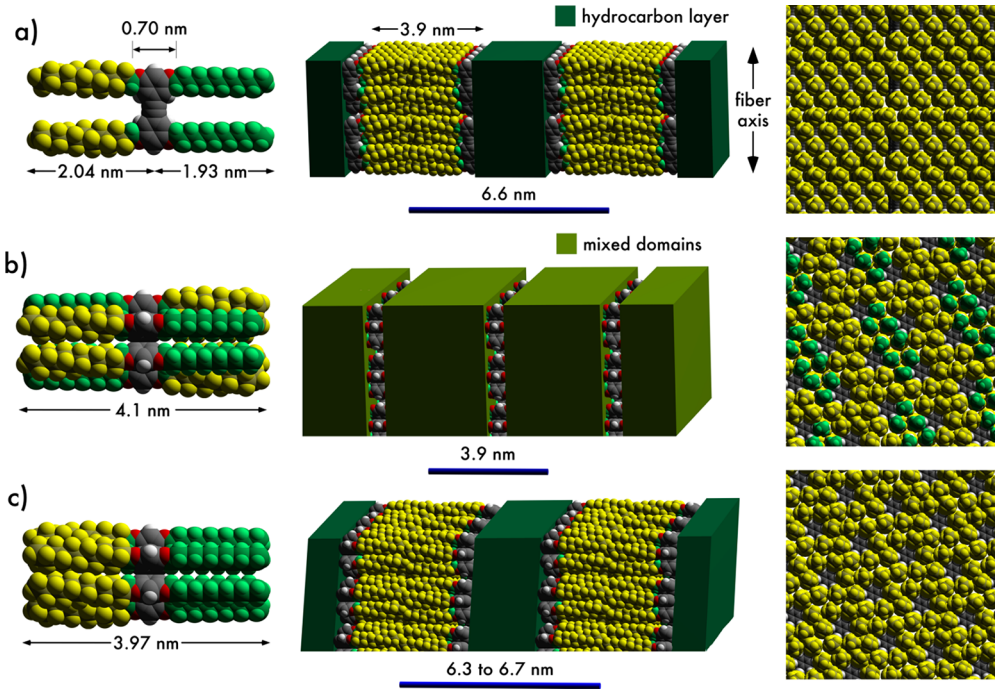

Figure 1. Chemical structure (left), molecular packing (middle), and fluorocarbon chain end (CF_3) view from a single molecular layer (right) for the tethered fluorous amphiphiles: (a) biphasic diphenylacetylene (DPA); (b) biphasic HPB, hexakis(3-(1-perfluoroundecylmethoxy)-5-dodecyloxyphenyl)benzene; (c) 1% DPA-doped biphasic HPB, shown at temperatures above 90 °C. The indicated distances are obtained from X-rays.

temperatures where the derivative of ε' has been employed ($d\varepsilon'/d \ln \omega \sim -(2/\pi)\varepsilon''$). This method is useful in fitting relaxation processes which are hidden under the conductivity, provided that the system is free of surface polarization effects. Therefore, the latter representation was employed in the analysis of the slower process. In addition, the characteristic times of ionic mobility were extracted using the electric modulus representation as $M^* = 1/\varepsilon^* = M' + iM''$. In this representation, the characteristic times for ion motion correspond to the crossing of the real and imaginary parts.[17]

Rheology. The viscoelastic properties were investigated with an advanced rheometric expansion system (ARES) equipped with a force-rebalanced transducer in the oscillatory mode. A parallel-plate geometry was used with a diameter of 25 mm and a thickness of about 0.5 mm. Two types of experiments were performed: (a) dynamic temperature rumps at 10 rad/s and (b) dynamic frequency sweeps at selected temperatures.

III. RESULTS AND DISCUSSION

Structure and Thermodynamic State. The results from the structural investigation reported in ref 13 are summarized in Figure 1. The figure depicts the packing in DPA that is based on the X-ray study (Figure 1a). The indicated periodicity of 6.6 nm results from a fluorocarbon bilayer that is expected by the "ideal" placement of the chains on the diphenylacetylene core and by a partially interdigitated or tilted hydrocarbon chains. Thus the structure consists of three pure domains composed of hydrocarbon chains, fluorocarbon chains, and diphenylacetylene cores. In addition to the X-ray study, the chemical shift of the ^{19}F CF_3 resonance, which is a sensitive probe of the chemical environment, could further elucidate the local packing, as observed through the terminal CF_3 groups. On the basis of the combined ^{19}F NMR and X-ray studies, the chemical structure viewed from a single molecular layer (Figure 1a) suggests a uniform environment and a dense packing of the CF_3 groups. This finding has consequences on the dynamics and will be discussed below.

The self-assembly in the biphasic HPB is considerably different (Figure 1b). A lateral periodicity of 3.9 nm shows a molecular lamellar spacing composed of mixed hydrocarbon and fluorocarbon chains. Because the fluorocarbon and hydrocarbon chains are incompatible, they are kinetically trapped. In addition, the CF_3 resonances in NMR were found to be distributed among all three environments with the majority in mixed domains. This situation for the packing of the CF_3 group with mixed chains within a single HPB molecule is visualized in the chemical structure viewed from a single molecular layer (Figure 1b).

Addition of only 1% DPA to the HPB affects the self-assembly especially at $T > 363$ K (Figure 1c). The X-ray scattering study revealed the formation of a supramolecular lamellar with a spacing of ca. 6.3 nm at 373 K. This distance reflects a fluorocarbon bilayer structure with complete interdigitation of hydrocarbon chains. Hence DPA unlocks the kinetically trapped conformation of HPB by facilitating the conversion between rotational isomers to the thermodynamically stable phase. At low temperatures, ^{19}F MAS NMR revealed that a significant portion of CF_3 remained in a mixed hydrocarbon/fluorocarbon phase. On heating, the CF_3 resonances from the mixed conformations were the first to melt, whereas the fluorocarbon bilayers melted last.

These structural features show also in the thermodynamics. Compared to pure HPB and DPA, additional transitions are evident in the DSC trace of the doped HPB, obtained on cooling and subsequent heating (Figure 2). The temperatures and associated heats of fusion are given in Table 1. In addition to these first-order transitions, a glass temperature at ~231 K

dx.doi.org/10.1021/jp309465z | J. Phys. Chem. B 2012, 116, 13812−13820

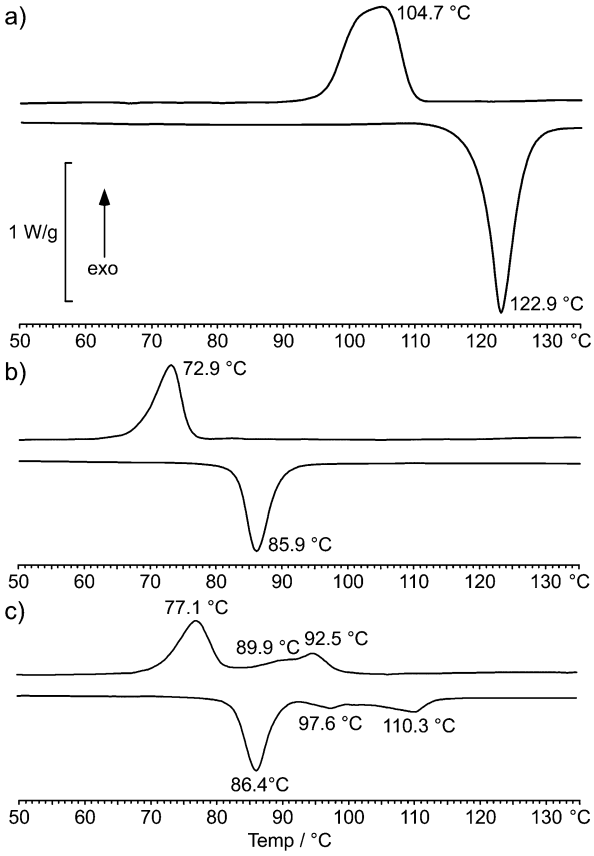

Figure 2. DSC traces obtained on cooling and subsequent heating (at 10 K/min) of the biphasic DPA (a), the pure biphasic HPB (b), and the 1% DPA-doped biphasic HPB (c).

Table 1. Thermal Properties and Phase Transitions of the 1% DPA-Doped Biphasic HPB

	temp of transformation (K)	heat of fusion (J/g)	phase transformation
cooling	366[b]	~5	isotropic to liquid-like fluorocarbon bilayer lamellar
	350[b]	9.1	liquid-like lamellar to solid lamellar
	231[a]		glass temperature
heating	231[a]		glass temperature
	360[b]	9.4	solid lamellar to liquid-like lamellar
	383[b]	3.8	liquid-like lamellar to isotropic

[a]From DS. [b]From DSC (10 K/min).

was identified on the basis of the results of the dynamic investigation (see Dynamics below). On the basis of the structural investigation, the transitions at 360 and 383 K correspond to the melting of the mixed lamellar structure and to the complete melting of the fluorocarbon bilayer, respectively.

This solid state structure of the HPB doped with 1% DPA is very different from the corresponding SFA, i.e., the $F_{12}H_{12}$, in that the high-temperature phase in the latter consists of a monolayer.[13] A bilayer structure best minimizes the fluorocarbon and hydrocarbon contacts and at the same time allows for the hydrocarbon segments to adjust their density, a consequence of hydrocarbon dynamics. Although the doped HPB assumes this preferred thermodynamic state, it remains unclear why this is not the case with SFAs.

Dynamics. The dielectric activity in fluorous compounds, like the ones investigated here, originates from the uncompensated terminal C−F dipole of the CF_3 group. This dipole should be very close to that of CH_3F (μ_{CH_3F} = 1.81 D). Figure 3 gives the dielectric loss under "isochronal" conditions

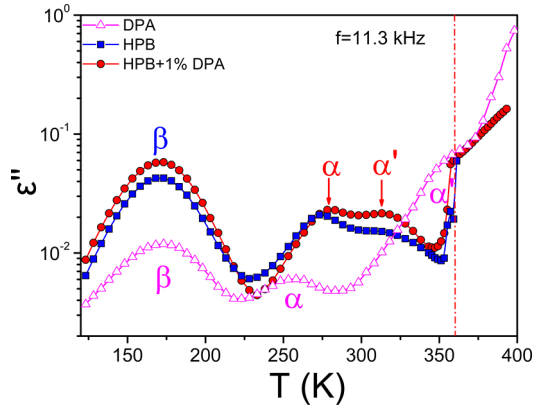

Figure 3. Dielectric loss under "isochronal" conditions for DPA (triangles), pure HPB (squares), and the 1% DPA-doped HPB (circles) obtained on heating at a frequency of 11.3 kHz. Greek letters indicate three relaxation processes (β, α, and α') originating from the C−F dipole. The vertical line signifies the melting of the defected structure in the HPB related compounds (T = 360 K).

for the three compounds. Three partially overlapping processes are evident in the dielectric loss curve indicated as β, α, and α' by increasing temperature. As we will discuss below, the process at lower temperatures (indicated as β) is the usual secondary process reflecting the restricted dipole motion within the glassy state. Its position is identical in the different compounds, suggesting small-amplitude motion of the end C−F dipole independent of the environment. Two processes are evident (called α and α') in the bulk HPB, doped HPB and in DPA. The abrupt increase of the dielectric loss at around 360 K reflects the unfreezing of the end-dipole relaxation upon melting of the defected structure in the HPB related compounds.

The viscoelastic response in the vicinity of the thermal and structural transitions was investigated with rheology. Figure 4 gives the storage (G') and loss (G'') shear moduli under "isochronal" conditions for the 1% DPA doped HPB in comparison to the dielectric loss. The figure depicts a solid-like response (with $G' > G''$) up to about 360 K. Taken together with the results from the X-ray investigation, the isochronal DS and DSC results suggest that the thermal transition at 360 K is a transformation from a *solid* lamellar structure, composed of mixed fluorocarbon and hydrocarbon chains, to a *liquid*-like lamellar phase composed of a liquid phase (based on ^{19}F NMR[13] and rheology) and a fluorocarbon bilayer lamellar. At T < 360 K, the two dielectrically active processes, α and α', also appear in the loss shear moduli as two shallow peaks. Apparently, the restricted dipolar C−F reorientation associated with the α and α' processes involves some intermolecular cooperativity, it couples to its environment and becomes mechanically active.

The dipolar relaxation for the 1% DPA-doped HPB can better be seen in Figure 5 under "isothermal" conditions. The

dx.doi.org/10.1021/jp309465z | J. Phys. Chem. B 2012, 116, 13812−13820

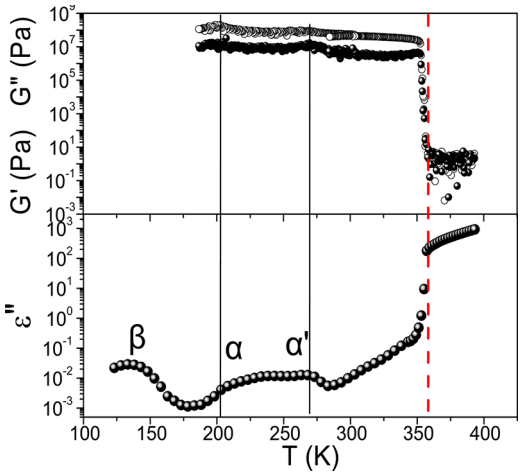

Figure 4. (Top) "Isochronal" measurements of the storage (open symbols) and loss (filled symbols) shear moduli corresponding to the 1% DPA-doped HPB, obtained at an angular frequency of 10 rad/s. (Bottom) "Isochronal" dielectric loss data obtained at a frequency of 1.59 Hz. The vertical dashed line (red) is associated with the melting of the defected structure whereas the two weak maxima in the loss modulus correspond to the two relaxations (α and α') found in DS. At lower temperatures, the β process is also contributing to the dielectric loss.

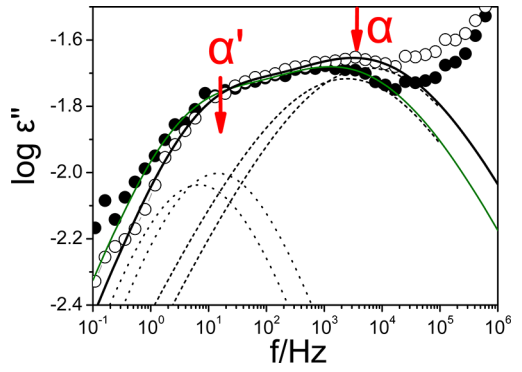

Figure 5. Frequency dependence of the dielectric loss spectra of the 1% DPA-doped HPB. The deconvolution of the two relaxation processes (α and α') is shown with dashed (α) and dotted (α') lines at two temperatures: 268 K (open circles) and 263 K (filled circles).

separation of the two overlapping processes, α and α', is best made in the frequency representation by employing two HN functions:

$$\varepsilon^*(\omega) = \varepsilon_\infty + \sum_{i=1}^{2} \frac{\Delta\varepsilon_i(\mathrm{T})}{[1 + (i\omega\tau_{i,\mathrm{HN}}(T))^{m_i}]^{n_i}} \quad (3)$$

with shape parameters $m = mn = 0.36$ and $m = mn = 0.52$ for the α and α' processes, respectively. The corresponding relaxation times and the associated dielectric strengths ($\Delta\varepsilon$) in the 1% DPA-doped HPB are shown in Figure 6 in the usual Arrhenius representation. The high-frequency/low-temperature β process was fitted to a single HN function (with low- and high-frequency shape parameters $m = 0.45$, $mn = 0.26$). It has an Arrhenius T dependence

$$\tau = \tau_0 e^{E/RT} \quad (4)$$

with a single activation energy $E = 35$ kJ/mol and a $\tau_0 \sim \times 10^{-15}$ s, characteristic of a local process. The α and α' processes have

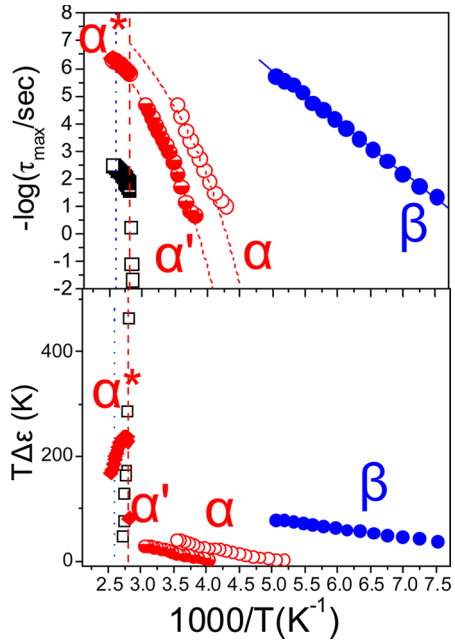

Figure 6. Relaxation map for the 1% DPA-doped HPB. (Top) Temperature dependence of the relaxation times corresponding to the β (filled circles), α (open circles), α' (half-filled circles), and the α* process (filled rhombus) at higher temperatures. Dashed lines represent VFT fits to the two processes. The vertical dashed and dotted lines give the transition temperatures from DSC that correspond to the melting of the defected lamellar structure (red) and the melting of the remaining fluorous bilayer (blue). The process due to the ionic mobility is also shown (open squares). (Bottom) T dependence of the dielectric strength ($T\Delta\varepsilon$) corresponding to each process.

a steeper temperature dependence that can be described by the Vogel–Fulcher–Tammann (VFT) equation:

$$\tau = \tau_0 \exp\left(\frac{B}{T - T_0}\right) \quad (5)$$

where B is the activation parameter and T_0 is the "ideal" glass temperature associated with the freezing of the dynamics at the glass temperature T_g (operationally defined as the temperature where $\tau \sim 10^2$ s). The B, T_0, and T_g parameters assume values of 410 ± 45, 182 ± 5, and 231 ± 3 K for the α and 1000 ± 120, 168 ± 8, and 246 ± 3 K for the α' process. The origin of the two partially overlapping processes can be discussed in terms of the local structure. The X-ray and ^{19}F NMR investigations, revealed that significant portion of CF_3 is in the solid lamellar composed of mixed hydrocarbon/fluorocarbon chains, especially at lower temperatures. A different local environment for the end C–F dipole is responsible for the two cooperative processes. For example, a conformational isomer that would mix one fluorocarbon chain with five hydrocarbon chains in one domain will inextricably lead to a domain having the opposite composition (Figure 1b). This creates a variation in local packing for the CF_3 groups that shows up as different dynamic processes. There are also similarities with the end dipole dynamics in poly(styrene-*b*-butadiene) copolymers[18] with fluorocarbon side chains that also display a bimodal relaxation with a VFT temperature dependence. This bimodal segmental mobility is also reminiscent of the dynamics of rod-like molecules with nematic order or with side-chain liquid crystalline polymers.[19,20] According to the theory of Martin,

dx.doi.org/10.1021/jp309465z | J. Phys. Chem. B 2012, 116, 13812–13820

Meier, and Saupe,[21] the splitting of the relaxation originates from the nematic potential with a magnitude that depends on the nematic order parameter. In the case of the side-chain liquid crystalline polymers it was shown that the slow process (called δ) is a sensitive probe of the order within the smectic layers.[19,20] In DPA, the highly ordered and well-packed fluorocarbon chains (Figure 1a) are expected to lead to the retardation of the slower (α') process.

On heating the sample, the melting of the solid lamellar has consequences on the dynamics. At $T > 360$ K, the dielectric signal increases abruptly. Within the temperature range $360 < T < 384$ K, a single process exists (α^*) with a VFT dependence (shape parameters $m = mn = 0.94$). This process corresponds to the CF_3 dynamics within the liquid-like lamellar and is in agreement with the low viscosity of the system (Figure 4). The characteristic time of ion mobility is also shown in the figure. Ionic mobility is retarded below 360 K but speeds up by several orders of magnitude at the melting temperature in contrast to the α^* that speeds-up only by 1 order of magnitude. This suggests that ionic impurities are able to move through a liquid phase that coexists with the fluorocarbon bilayer lamellar.

Figure 7 compares the dynamics in the different compounds and within the different environments. The β process with

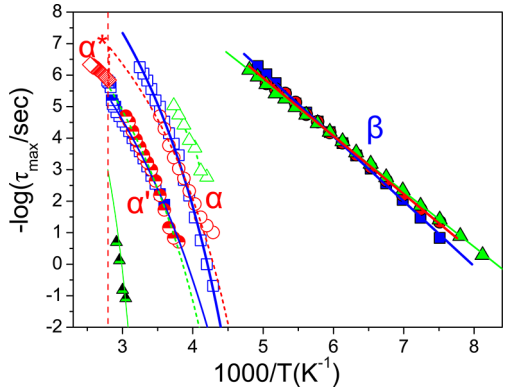

Figure 7. Temperature dependence of the relaxation times corresponding to the β (filled symbols), α (open symbols), α' (half-filled symbols), and α^* process (open rhombus) of DPA (triangles), HPB (squares), and the 1% DPA-doped HPB (circles). The lines are fits to the Arrhenius (β process) or VFT (α and α') equations. The vertical line corresponds to the melting temperature of the defected lamellar structure in the HPB-related compounds.

nearly identical activation energy is found in all compounds, suggesting the same low-amplitude dipolar relaxation. The similarity in the α and α' processes in the pure and doped HPB at $T < 360$ K nicely reflects the similar (mixed) environment of the fluorocarbon chains. This is in agreement with the ^{19}F NMR study (Figure 1b), probing the same CF_3 groups. On the other hand, the dynamics of DPA forming pure fluorocarbon bilayers is different. The α' process is much slower reflecting the higher order within the uniform fluorocarbon bilayers.

Pressure Dependence. The advantage of employing pressure is 2-fold: first, it can elucidate the origin of the dynamic processes, and second, it is a necessary variable for the construction of the equilibrium phase diagram (i.e., $T-P$ diagram[22−24]). In these experiments, pressure is applied isothermally at temperatures where the α^* process is probed within the experimental window. The results for the relaxation times and the associated dielectric strengths are depicted in Figure 8 for several "isotherms". The effect of pressure is to slow-down the dynamics of the α^* process and to increase its

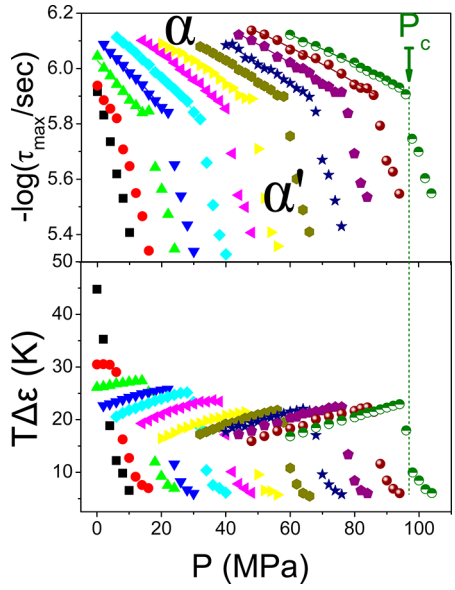

Figure 8. (Top) Pressure-dependent relaxation times for the 1% DPA-doped HPB corresponding to the transformation of the high-temperature α^* process within the liquid-like fluorous bilayer lamellar to the solid lamellar (process α') under isothermal conditions: (squares) 363 K; (circles) 368 K; (up triangles) 373 K; (down triangles) 378 K; (rhombi) 383 K; (left triangles) 388 K; (right triangles) 393 K; (hexagons) 398 K; (stars) 403 K; (pentagons) 408 K; (spheres) 413 K; (half-filled circles) 418 K. (Bottom) Corresponding dielectric strengths plotted as $T\Delta\varepsilon$. The discontinuous change of the relaxation times and of the associated intensities signify the critical pressure (P_c) at the transition.

dielectric strength. The increase in the dielectric strength can be expressed by the Fröhlich equation for spherical molecules[14] as

$$\Delta\varepsilon = \frac{4\pi N_A \rho g \mu^2}{3k_B T M_0} F \tag{6}$$

where N_A is the Avogadro number, ρ is the mass density, g is a measure of the orientational pair correlations ($g = 1 + z\langle\cos\theta\rangle$, z is the average number of nearest neighbors, and θ is the angle between neighbors), μ is the dipole moment, M_0 is the molecular weight, and F is the local field correction. Increasing pressure results in the increase of $\Delta\varepsilon$ mainly through densification. Further increase of pressure beyond a critical value, P_c, results in the formation of the solid lamellae under isothermal conditions as evidenced by the steep increase in the relaxation times (α') and the simultaneous loss in dielectric strength. This is to be expected because increasing pressure under isothermal conditions favors the more dense lamellar phase associated with the α' process. The approximately linear dependence of $\log\tau$ vs pressure at $P < P_c$ can be used to define an apparent activation volume, $\Delta V^{\#}$, as[15,25]

$$\Delta V^{\#} = 2.303 \cdot RT \left(\frac{\partial \log \tau}{\partial P} \right)_T \tag{7}$$

This quantity is plotted in Figure 9 as a function of temperature. $\Delta V^{\#}$ in many amorphous systems assumes values that are comparable to the monomer volume (M_0/ρ).[15,25,26] Assuming a density of 1.5 g/cm^3 gives a monomer volume of

dx.doi.org/10.1021/jp309465z | J. Phys. Chem. B 2012, 116, 13812−13820

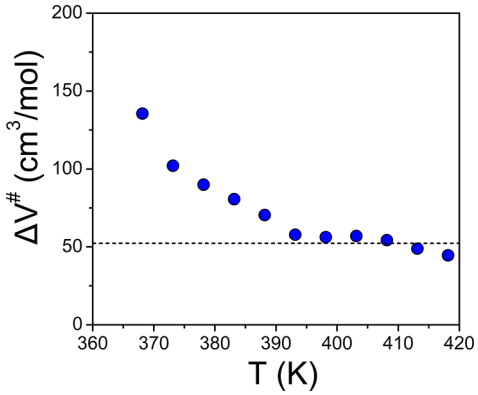

Figure 9. Temperature dependence of the apparent activation volume corresponding to the α^* process at $P < P_c$. The dashed line gives the corresponding volume of a single CF_3 group.

~3500 g/mol, which is much higher than the apparent activation volume of the process. However, what is probed under these T and P conditions is not the reorientation motion of the molecule as a whole, but restricted small amplitude motions of the terminal C−F dipole. In addition, $\Delta V^{\#}$ is temperature dependent, reaching a value of ~50 cm^3/g at higher temperatures. This value is comparable to the molecular volume of a single CF_3 group. This reflects a cooperative C−F dipole relaxation that on increasing temperature loses cooperativity and becomes intramolecular.

Equilibrium Phase Diagram. The T- and P-dependent dynamics in the 1% DPA-doped HPB allows for the construction of the "equilibrium" phase diagram[22−25] depicted in Figure 10. Four phases are shown (three equilibrium phases and one nonequilibrium phase). Starting from high temperature, one finds the isotropic phase (presumably with the same α^* dielectric process; the dynamics cannot be studied due to the experimentally available frequency range); the liquid-like fluorocarbon bilayer lamellar phase, composed of nanophase-separated fluorocarbon and hydrocarbon domains (with a single α^* process); the solid lamellae composed of mixed fluorocarbon and hydrocarbon chains (with two relaxation processes α and α' both reflecting different C−F end-dipole environments); and a "frozen" (i.e., glassy) phase at lower temperatures (below which a single β process exists). The single point for the isotropic phase (open squares) was obtained from DSC at ambient pressure, whereas all remaining points are obtained from DS at ambient and at elevated pressures. The experimental (T, P) points (open circles in Figure 10) reflecting the transformation between the two lamellar phases were obtained by using the (T, P_c) points marking the onset of phase transformation (Figure 8). The resulting linear $T(P)$ dependence conforms to the Clausius−Clapeyron equation:

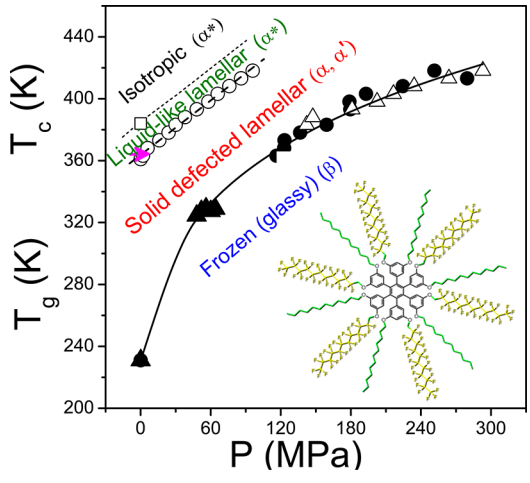

Figure 10. Phase diagram for the 1% DPA-doped HPB displaying the phase and the corresponding dynamic processes (in parentheses). The single point for the isotropic phase (open square) is obtained from DSC whereas all remaining points are from DS as follows: (open circles) critical pressures from Figure 8; (open triangles) α^* extrapolated "isothermal" measurements to T_g (defined at $\tau \sim 1$ s) from Figure 8; (filled triangles) α^* extrapolated "isobaric" points; (filled circles) α' extrapolated "isothermal" measurements. The horizontal arrow indicates the pressure jump experiments used in the investigation of the kinetics and is explained in the text.

$$\frac{dP}{dT} = \frac{\Delta H}{T\Delta V} \tag{8}$$

where ΔH is the heat of fusion and ΔV the change of volume at the transition. Using T = 360 K, dP/dT = 1.7 MPa/K and the measured ΔH = 9 J/g (Table 1) results in a change of volume of 0.015 cm^3/g. This is a reasonable estimate given existing PVT measurements on systems composed of semifluorinated alkane composites.[27] The experimental $T_g(P)$ points are obtained by extrapolating the "isothermal" and "isobaric" times of the corresponding α^* process to temperatures where the relaxation time is at 1 s. This certainly involves a large extrapolation; nevertheless, it is included (Figure 10) to delineate the boundaries between the solid lamellar phase and the "frozen" glassy phase. The $T_g(P)$ dependence can be parametrized according to the empirical equation[28]

$$T_g(P) = T_g(0)\left(1 + \frac{\kappa}{\lambda}P\right)^{1/\kappa} \tag{9}$$

where $T_g(0)$ refers to the glass temperature at atmospheric pressure and κ = 6.3 and λ = 41 MPa. The initial slope $(dT_g/dP)_{P\to 0}$ being equal to $T_g(0)/\lambda$ amounts to 5.6 K/MPa. At temperatures below the dynamic $T_g(P)$, a single process exists into the glassy state (the β process).

Kinetics of Phase Transformation. Knowledge of the equilibrium phase diagram of the 1% DPA-doped HPB permits the investigation of the kinetics of the liquid-to-solid lamellar transformation. This can best be studied under "isothermal" conditions by performing pressure-jump experiments[29] to P_c, which drives the system from the liquid-like lamellar to the solid lamellar phase (Figure 10, horizontal arrow). The result for the dielectric loss following a pressure jump from 0.1 to 11.5 MPa at T = 368 K is shown in Figure 11. The data shown with square symbols correspond to the dielectric loss at 368.15 K and at atmospheric pressure. The "isothermal/isobaric" data, depicted with the filled circles, correspond to the dielectric loss immediately following the pressure-jump to 11.5 MPa (defined as t = 0 s). The remaining loss curves correspond to later times under the same T and P_c conditions. As expected, the dielectric strength of the process is reduced during the transformation to the solid lamellar phase, reflecting the reduction in the amplitude of motion of mobile dipoles. The evolution of $\Delta\varepsilon(t)$, shown in the inset, can be represented by the Kohlrausch−Williams−Watts (KWW) equation

dx.doi.org/10.1021/jp309465z | J. Phys. Chem. B 2012, 116, 13812−13820

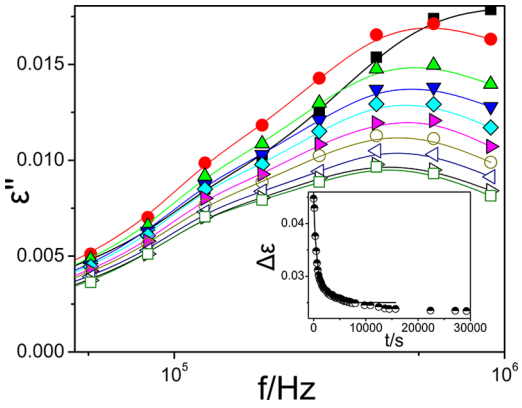

Figure 11. Dielectric loss as a function of frequency following the kinetics of the phase transformation from the α^* to α' process associated with the structural transition from the fluorous bilayer lamellar to the defected lamellar in the 1% DPA-doped HPB. All spectra are obtained at 368 K by following a pressure jump from atmospheric pressure to 11.5 MPa (arrow in Figure 10). The different symbols correspond to different times as follows: (filled squares) atmospheric pressure, (filled circles) immediately after the pressure jump to 11.5 MPa defined as t = 0; (filled up triangles) t = 165 s; (filled down triangles) t = 323 s; (filled rhombus) t = 480 s; (filled right triangles) t = 800 s; (open circles) t = 1450 s; (open left triangles) t = 3737 s; (open right triangles) t = 9615 s; (open squares) t = 69124 s. In the inset, the evolution of the dielectric strength is shown together with the result of the fit to eq 10.

$$\Delta\varepsilon = A\,\exp\left[-\left(\frac{t-t_0}{\tau^*}\right)^{\nu}\right] + c \qquad (10)$$

where A is the amplitude, t_0 an initial time required for temperature equilibration, τ^* the characteristic crystallization time, and ν is the KWW exponent. The values of the exponent ν are consistently below 1, and this contrasts with the exponents encountered during polymer crystallization.[30] The latter conform to the Avrami equation[31] and the exponent ν reflects the type of nucleation process and the dimensionality of growth. The lower values of the exponent (ν = 0.53 at T = 368 K) suggest that formation of the solid lamellar phase is a highly cooperative process. This is anticipated as the transformation requires solidification and internal reorganization by mutual rotation of the fluorocarbon and hydrocarbon chains followed by adjustment of their density.

The effect of the depth of the pressure jump (i.e., pressure "quench") on the phase transformation is explored in Figure 12, where the evolution of the dielectric strength is plotted following pressure jumps to different final pressures at 388 K. In general, the deeper the pressure-quench to the new equilibrium phase, the higher the driving force ($\delta \sim (P - P_c)/P_c$) and the corresponding intensity drop and the faster the kinetics. The average times, obtained by applying eq 10 to the data (Figure 12, inset) ($\langle\tau\rangle = (\tau^*/\nu)\Gamma(1/\nu)$, where Γ is the gamma function), exhibit a drastic reduction by increasing driving force. This type of pressure-quench experiments could be further employed in determining the stability limits (i.e., spinodals) of the equilibrium phases, but this is beyond the scope of the present study. Nevertheless, the kinetic experiments suggest a nucleation and growth mechanism for the solid lamellar phase that involves synergy in conformational changes.

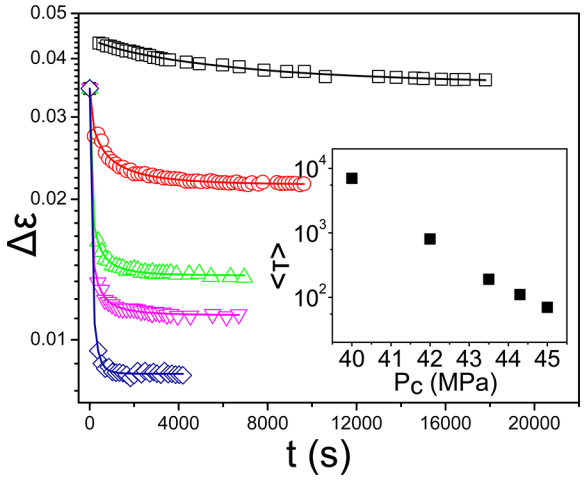

Figure 12. Evolution of the dielectric strength for the 1% DPA-doped HPB obtained at 388 K following pressure jumps to 40 MPa (squares), 42 MPa (circles), 43.5 MPa (up triangles), 44.3 MPa (down triangles), and 45 MPa (rhombus). The lines are fits to eq 10. In the inset, the dependence of the average kinetic times is shown as a function of the final pressure.

IV. CONCLUSIONS

Tethering of incommensurate hydrocarbon and fluorocarbon side chains to the rotationally flexible HPB core leads to a rich self-assembly that is distinctly different from the analogous SFAs. This gives rise to different packing motifs for the CF_3 groups. The end C−F dipole of the CF_3 group has been employed as a sensitive probe of the local environment within the different phases.

In the *dynamics*, four dielectrically active processes, in addition to the ionic mobility, exist within the different phases. These reflect (i) a localized process with an Arrhenius temperature dependence within the glassy state, (ii) two processes above T_g with a strong (VFT) temperature (and pressure) dependence within the solid lamellar phase composed of a mixed fluorocarbon and hydrocarbon layers and (iii) a high-temperature process reflecting the dipole reorientation within the liquid-like fluorocarbon bilayer lamellar phase. The *equilibrium phase diagram* was established by pressure-dependent studies. Three equilibrium phases that correspond to the structural investigation and one non-equilibrium (glassy) phase exist. The transformation between the two lamellar phases conforms to the Clausius−Clapeyron equation anticipated by the nature of the transition (first order). From the pressure coefficient of the transition, the change of volume associated with the transformation was estimated as 0.015 cm^3/g. The *kinetics* of phase transformation from the liquid-like fluorocarbon bilayer lamellar to the solid lamellae was followed by pressure-quench experiments. The stretched exponential relaxation and the strong dependence of the characteristic times on pressure suggest that the phase transformation between the liquid and solid lamellae is a highly cooperative process, atypical for nucleation and growth. The increased cooperativity is discussed in terms of the mutual intramolecular rotation of the fluorocarbon and hydrocarbon chains.

In this propeller-like molecule, synergistic conformational changes are held responsible for the slow dynamics and kinetics. Yet the latter do not prevent the system from reaching the preferred thermodynamic state in contrast to SFAs.

dx.doi.org/10.1021/jp309465z | J. Phys. Chem. B 2012, 116, 13812−13820

Molecular complexity may create pathways toward equilibrium. We are currently exploring this issue in other fluorocarbon/hydrocarbon amphiphiles.

AUTHOR INFORMATION

Corresponding Author

*E-mail: gfloudas@cc.uoi.gr.

Present Address

[§]University of Leipzig, Institute of Experimental Physics 1, D-04103 Leipzig, Germany.

Notes

The authors declare no competing financial interest.

ACKNOWLEDGMENTS

GF acknowledges support during his sabbatical leave at the MPI-P. The current work was supported by the Research unit on Dynamics and Thermodynamics of the UoI cofinanced by the European Union and the Greek state under NSRF 2007-2013 (Region of Epirus, call 18). This work was cofinanced by the E.U.- European Social Fund and the Greek Ministry of Development - GSRT in the framework of the program THALIS. Financial support by DFG Priority Program SPP1355, SFP 1459 and the SFB635 is acknowledged. C.G.C. is grateful for financial support from a U.S. National Science Foundation MPS Distinguished International Research Fellowship (MPS-DRF) (Award: DMR- 0207086) and from the Max Planck Society. The authors would like to thank Sunna Scholz for synthetic support.

REFERENCES

(1) Riess, J. G. *Tetrahedron* **2002**, *58*, 4113−4131.
(2) Rabolt, J. F.; Russell, T. P.; Twieg, R. J. *Macromolecules* **1984**, *17*, 2786−2794.
(3) Russell, T. P.; Rabolt, J. F.; Twieg, R. J.; Siemens, R. L.; Farmer, B. L. *Macromolecules* **1986**, *19*, 1135−1143.
(4) Viney, C.; Russell, T. P.; Lepero, L. E.; Twieg, R. J. *Mol. Cryst. Liq. Cryst.* **1989**, *168*, 63−82.
(5) Höpken, J.; Möller, M. *Macromolecules* **1992**, *25*, 2482−2489.
(6) Höpken, J.; Pugh, C.; Richtering, W.; Möller, M. *Makromol. Chem.* **1988**, *189*, 911−925.
(7) Nostro, P. L.; Chen, S.-H. *J. Phys. Chem.* **1993**, *97*, 6535−6540.
(8) Marczuk, P.; Lang, P. *Macromolecules* **1998**, *31*, 9013−9018.
(9) Song, K.; Hallmark, V. M.; Rabolt, J. F. *J. Chem. Phys.* **1991**, *95*, 2862−2866.
(10) Rabolt, J. F.; Fanconi, B. *Polymer* **1977**, *18*, 1258−1264.
(11) Núñez, E.; Clark, C. G.; Cheng, W.; Best, A.; Floudas, G.; Semenov, A. N.; Fytas, G; Müllen, K. J. *Phys. Chem. B* **2008**, *112*, 6542−6549.
(12) Semenov, A. N.; González-Pérez, A.; Krafft, M. P.; Legrand, J.-F. *Langmuir* **2006**, *22*, 8703−8717.
(13) Clark, C. G.; Floudas, G. A.; Lee, Y. J.; Graf, R.; Spiess, H. W.; Müllen, K. *J. Am. Chem. Soc.* **2009**, *131*, 8537−8547.
(14) Kremer, F.; Schönhals, A. *Broadband Dielectric Spectroscopy*; Springer: Berlin, 2002.
(15) Floudas, G.; Paluch, M.; Grzybowski, A.; Ngai, K. L. *Molecular Dynamics of Glass-Forming Systems. Effects of Pressure*; Springer: Berlin, 2011.
(16) Havriliak, S.; Negami, S. *Polymer* **1967**, *8*, 161−210.
(17) Floudas, G. In *Dielectric Spectroscopy.*; Matyjaszewski, K., Möller, M., Eds.; Polymer Science: A Comprehensive Reference, Vol. *2.32*; Elsevier BV: Amsterdam, 2012; pp 825−845.
(18) Floudas, G.; Antonietti, M.; Förster, S. *J. Chem. Phys.* **2000**, *113*, 3447−3451.
(19) Schönhals, A.; Wolff, D.; Springer, J. *Macromolecules* **1998**, *31*, 9019−9025.
(20) Floudas, G.; Mierzwa, M.; Schönhals, A. *Phys. Rev. E* **2003**, *67*, 031705 1−8.
(21) Maier, W.; Meier, G.; Saupe, A. *Faraday Symp. Chem. Soc.* **1975**, *5*, 119−126.
(22) Mierzwa, M.; Floudas, G.; Stepanek, P.; Wegner, G. *Phys. Rev. B* **2000**, *62*, 14012−14019.
(23) Gitsas, A.; Floudas, G.; Wegner, G. *Phys. Rev. E* **2004**, *69*, 041802 1−8.
(24) Haase, N.; Grigoriadis, C.; Butt, H.-J.; Müllen, K.; Floudas, G. *J. Phys. Chem. B* **2011**, *115*, 5807−5814.
(25) Floudas, G. *Prog. Polym. Sci.* **2004**, *29*, 1143−1171.
(26) Floudas, G.; Gravalides, C.; Reisinger, T.; Wegner, G. *J. Chem. Phys.* **1999**, *111*, 9847−9852.
(27) Gottwald, A.; Pospiech, D.; Jehnichen, D.; Haussler, L.; Friedel, P.; Stamm, M.; Floudas, G. *Macromol. Chem. Phys.* **2002**, *203*, 854−861.
(28) Andersson, S.; Andersson, O. *Macromolecules* **1998**, *31*, 2999−3006.
(29) Mierzwa, M.; Floudas, G. *IEEE Trans. Diel. EI* **2001**, *8*, 359−364.
(30) Wunderlich, B. *Macromolecules Physics 2. Crystallization, Nucleation, Growth, Annealing*; Academic Press: New York, 1978.
(31) Avrami, M. J. *J. Chem. Phys.* **1939**, *7*, 1103−1112; **1940**, *8*, 212−224; **1941**, *9*, 177−184.